Efficiency Improvement of Multichannel LED Driver With Selective Dimming

Cikai Ye, *Student Member, IEEE*, Hao Wei Chan, Dongdong Lan, *Student Member, IEEE*, Pritam Das, *Senior Member, IEEE*, and Sanjib Kumar Sahoo, *Senior Member, IEEE*

***Abstract*—There is a widespread application of selective dimming of multichannel LED drivers. In this article, two new selective dimming methods to improve the efficiency of multichannel LED drivers are proposed. The proposed methods are based on a two-stage multichannel LED driver that consists of an ac–dc boost power factor correction converter at its front-end and a dc–dc non-resonant converter at its second stage. Primary side digital peak current control method is applied to the dc–dc converter to control the LED peak currents during selective dimming operation. The auxiliary back-to-back switches are connected across each transformer winding either at the primary side or secondary side to perform selective dimming. The duty ratios of these auxiliary back-to-back switches are varied at lower than switching frequency of dc–dc converter to control the brightness of LED loads. The proposed topologies offer high efficiencies in both full load and during selective dimming operations, and meet the IEEE 1789 recommendation with 3 kHz dimming frequency. The design of the proposed dc–dc converters, modes of operation as well as detailed theoretical analysis are presented in this article. A 150-W prototype of the proposed LED driver with a non-DSP microcontroller is implemented to verify the feasibility of such LED drivers. Comparisons between the proposed methods and the converters reported previously are presented in the article.**

***Index Terms*—multichannel LED driver, primary side peak current control, selective dimming, shorting transformer windings.**

NOMENCLATURE

$i_{\rm pri}$	Primary side current.
$I_{\rm pri,pk}$	Peak value of $i_{\rm pri}$.
$f_{\rm SW}$	Switching frequency of primary side switches S_1 and S_2.
$f_{\rm dim}$	Dimming frequency.
$V_{\rm DC}$	Intermediate dc bus voltage.
V_o	Output voltage for each LED channel.
I_o	Output current for each LED channel.
$v_{\rm pri,T1}$	Voltage of primary side winding of transformer *T1*.
$v_{\rm pri,T2}$	Voltage of primary side winding of transformer *T2*.
$v_{\rm sec,T1}$	Voltage of secondary side winding of *T1*.
$v_{\rm sec,T2}$	Voltage of secondary side winding of *T2*.
$L_{\rm lk}$	Inductance of primary side leakage inductor.
N	Turns ratio of *T1* and *T2*.
$V_{\rm o(1\text{-}4)avg}$	Average output voltage of LED channels *CH1*–*CH4* in Group 1.
$V_{\rm o(5\text{-}8)avg}$	Average output voltage of LED channels *CH5*–*CH8* in Group 2.
$i_{\rm sec1}$	Current of secondary side winding of *T1*.
$i_{\rm sec2}$	Current of secondary side winding of *T2*.
$\lvert i_{\rm pri}\rvert_{avg}$	Average value of rectified $i_{\rm pri}$.
$\lvert i_{\rm sec1}\rvert_{\rm avg}$	Average value of rectified $i_{\rm sec1}$.
$\lvert i_{\rm sec2}\rvert_{\rm avg}$	Average value of rectified $i_{\rm sec2}$.
$I_{\rm avg,G1}$	Average LED current of Group 1.
$I_{\rm avg,G2}$	Average LED current of Group 2.
$D_{\%1}$	Dimming percentage of LED Group 1.
$D_{\%2}$	Dimming percentage of LED Group 2.
$D_{\rm pri}$	Operating duty ratio of S_1 and S_2.
$D_{\rm G1}$	Duty ratio of back-to-back switch $S_{\rm G1}$.
$D_{\rm G2}$	Duty ratio of back-to-back switch $S_{\rm G2}$.
$R_{\rm DSon,pri}$	ON-state resistance of S_1 and S_2.
$t_{f,\rm pri}$	Fall time of S_1 and S_2.
$f_{\rm SW,no}$	Switching frequency of S_1 and S_2 in state of no dimming.
$f_{\rm SW,one}$	Switching frequency of S_1 and S_2 in state of one-group dimming.
V_F	Forward voltage of secondary side rectifier diodes.
R_{Llk}	Resistance of series inductor winding.
$\Delta B_{\rm no}$	Peak ac flux density at no dimming switching frequency.
$\Delta B_{\rm one}$	Peak ac flux density at one-group dimming switching frequency.
k_{fe}	Core loss coefficient.
A_e	Core cross-sectional area.
l_m	Core magnetic path length.
$R_{\rm pri}$	Resistance of primary side winding of *T1* and *T2*.
$R_{\rm sec}$	Resistance of secondary side winding of *T1* and *T2*.
$R^{\rm pri}_{\rm DSon,SG}$	ON-state resistance of $S_{\rm G1}$ and $S_{\rm G2}$ for primary side shorting.

Manuscript received April 26, 2019; revised July 17, 2019 and September 20, 2019; accepted October 25, 2019. Date of publication November 4, 2019; date of current version February 20, 2020. This work was supported in part by the Singapore Ministry of National Development and the National Research Foundation, Prime Minister's Office, under the Land and Liveability National Innovation Challenge (L2 NIC) Research Programme under L2 NIC Award L2NICCFP2-2015-3, and in part by Republic of Singapore's National Research Foundation through a grant to the Berkeley Education Alliance for Research in Singapore for the Singapore-Berkeley Building Efficiency and Sustainability in the Tropics Program. Recommended for publication by Associate Editor J. M. Alonso. *(Corresponding authors: Cikai Ye; Pritam Das.)*

C. Ye, H. W. Chan, D. Lan, and S. K. Sahoo are with the Department of Electrical and Computer Engineering, National University of Singapore, Singapore 119077, Singapore (e-mail: cikai.ye@u.nus.edu; e0032099@u.nus.edu; landongdong@u.nus.edu; elesahoo@nus.edu.sg).

P. Das is with the Department of Electrical and Computer Engineering, State University of New York, Binghamton, NY 13902 USA (e-mail: pdas@binghamton.edu).

Color versions of one or more of the figures in this article are available online at http://ieeexplore.ieee.org.

Digital Object Identifier 10.1109/TPEL.2019.2951629

$R^{\rm sec}_{\rm DSon,SG}$	ON-state resistance of $S_{\rm G1}$ and $S_{\rm G2}$ for secondary side shorting.
$C^{\rm pri}_{\rm OSS}$	Output capacitance of $S_{\rm G1}$ and $S_{\rm G2}$ for primary side shorting.
$C^{\rm sec}_{\rm OSS}$	Output capacitance of $S_{\rm G1}$ and $S_{\rm G2}$ for secondary side shorting.
$t^{\rm pri}_{r,\rm SG}$	Rise time of $S_{\rm G1}$ and $S_{\rm G2}$ for primary side shorting.
$t^{\rm sec}_{r,\rm SG}$	Rise time of $S_{\rm G1}$ and $S_{\rm G2}$ for secondary side shorting.
$t^{\rm pri}_{f,\rm SG}$	Fall time of $S_{\rm G1}$ and $S_{\rm G2}$ for primary side shorting.
$t^{\rm sec}_{f,\rm SG}$	Fall time of $S_{\rm G1}$ and $S_{\rm G2}$ for secondary side shorting.
$\Delta P_{\rm loss}$	Total power loss difference between primary side shorting and secondary side shorting.
$\Delta P_{{\rm Cu},T}$	Difference of copper loss of *T1* and *T2*.
$\Delta P_{\rm cSG}$	Difference of conduction loss of $S_{\rm G1}$ and $S_{\rm G2}$.
$\Delta P_{\rm swSG}$	Difference of switching loss of $S_{\rm G1}$ and $S_{\rm G2}$.
$P^{\rm sec}_{{\rm Cu},T}$	Copper loss of *T1* and *T2* for secondary side shorting.
$P^{\rm pri}_{{\rm Cu},T}$	Copper loss of *T1* and *T2* for primary side shorting.
$P^{\rm sec}_{\rm cSG}$	Conduction loss of $S_{\rm G1}$ and $S_{\rm G2}$ for secondary side shorting.
$P^{\rm pri}_{\rm cSG}$	Conduction loss of $S_{\rm G1}$ and $S_{\rm G2}$ for primary side shorting.
$P^{\rm sec}_{\rm swSG}$	Switching loss of $S_{\rm G1}$ and $S_{\rm G2}$ for secondary side shorting.
$P^{\rm pri}_{\rm swSG}$	Switching loss of $S_{\rm G1}$ and $S_{\rm G2}$ for primary side shorting.
$i_{\rm G1}$	LED current of Group 1.
$i_{\rm G2}$	LED current of Group 2.
$i_{\rm pri,T1}$	Current of primary side winding of *T1*.
$P_{\rm auxLoss}$	Auxiliary power loss from output capacitators during selective dimming.
m	Number of dimming groups.
C_o	Output capacitance of each dimming group.
V_G	Output voltage of each dimming group.

I. Introduction

LED lighting is being widely used because of its high efficiency as compared to incandescent bulbs and fluorescent lights [1]. LED drivers are required for LEDs to operate properly with dc current but most applications require the drivers to be operated from 90 to 264 V ac input. To further increase the efficiency and reduce cost, multichannel LED drivers are developed to replace single-channel LED drivers. Additionally, multichannel LED drivers can operate at different brightness for each individual LED channel. This enables lighting applications to be more optimized as compared to the use of single-channel LED drivers. Hence, this leads to the emergence of multichannel selective dimming LED drivers.

Several multichannel selective dimming LED drivers are proposed in [2]–[18]. In [2], the proposed method uses separate converters to achieve selective dimming, which reduces efficiency due to multiple stages of energy conversion. In addition, there is an increased cost due to large number of components required for each individual LED channel.

In [3]–[8], the proposed non-isolated selective dimming LED drivers are used in low voltage and low power applications. According to UL standard [19], galvanic isolation is needed for ac input and high-power use. Thus, since there is a need to add one more stage of power conversion, the efficiency is reduced, and the cost is increased. In [9], the use of single-switch based isolated flyback converter with auxiliary buck/boost stage for selective dimming of LED channels is proposed. However, in high-power applications, the efficiency is greatly reduced due to hard-switching and large leakage inductance losses.

In [10] and [11], the selective dimming and current balancing by using switch-controlled capacitor-based LED drivers are proposed. For these two methods, the secondary side of transformers requires complicated control and the circuits consist of both active and passive components in every LED channel, leading to reduced efficiency. The isolated forward converters, which achieve current balancing in multichannel LED drivers using magnetic amplifier control, are presented in [12] and [13]. For every LED channel, an auxiliary bulky inductor is required for the control and current balancing. Hence, there will be higher power loss as well as reduced efficiency with increased input power and selective dimming levels of LEDs.

In [14] and [15], a method of variable inductance control is applied to realize selective dimming. However, this method leads to lower power density due to two-winding bulky variable inductors, and lower efficiency due to higher loss of variable inductors. The selective dimming function in [16] is realized by an additional buck stage with control IC applied on the secondary side of the transformer in each LED channel.

Another selective dimming LED driver is proposed in [17] and [18] which is based on the primary side peak current control method. This control method maintains the LED peak currents to prevent overcurrent from occurring, which will otherwise lead to electro-migration and hence fast-aging of LEDs [20]. The proposed topology in [17] also achieves current balancing in each channel by using symmetric quadrupler rectifiers. In this solution, the secondary side switches are positioned to be at each LED channel output to achieve selective dimming by varying their duty ratios. However, with increased dimming frequency and number of dimming groups, the efficiency of the LED driver will drop significantly. This is due to the energy loss through the discharge of capacitors during the transition at every ON state of the secondary side switches.

In this article, two new topologies to achieve better efficiency in selective dimming operations are proposed. These topologies are based on the multichannel equivalent dimming LED driver in [21]. The application of symmetric quadrupler rectifiers is remained for the proposed topologies because of its function of current balancing for all LED channels, less voltage stresses in diodes as well as reduced number of transformer windings at the secondary side [22]. The method based on the back-to-back switches is proposed for the high-efficiency isolated resonant converter in [23]. Similarly, the new proposed topologies use back-to-back switches that are connected in parallel to each respective transformer winding at primary side or secondary side. These topologies avoid the energy loss due to discharge of capacitors during the transition at every switching cycle in [17],

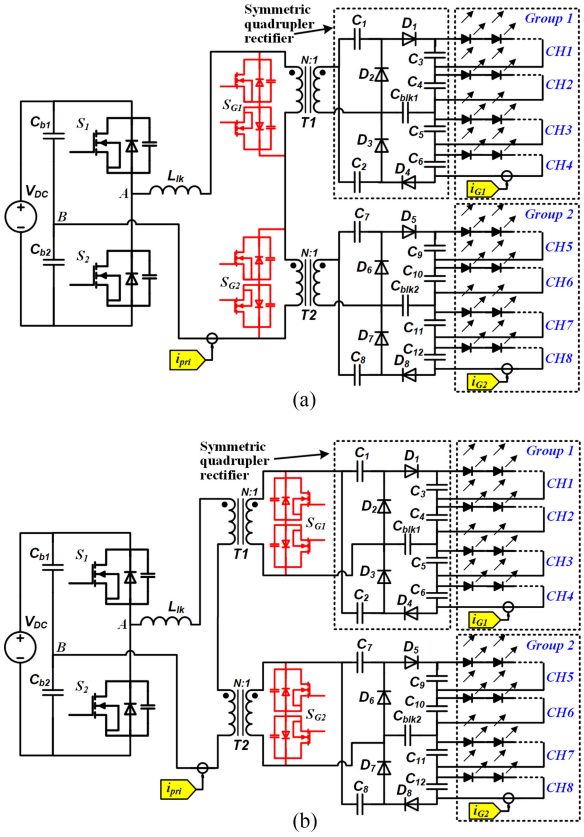

Fig. 1. Proposed topologies for selective dimming based on isolated dc–dc non-resonant converter by back-to-back switches placed in parallel with each respective transformer winding (a) at the primary side shorting and (b) at the secondary side shorting.

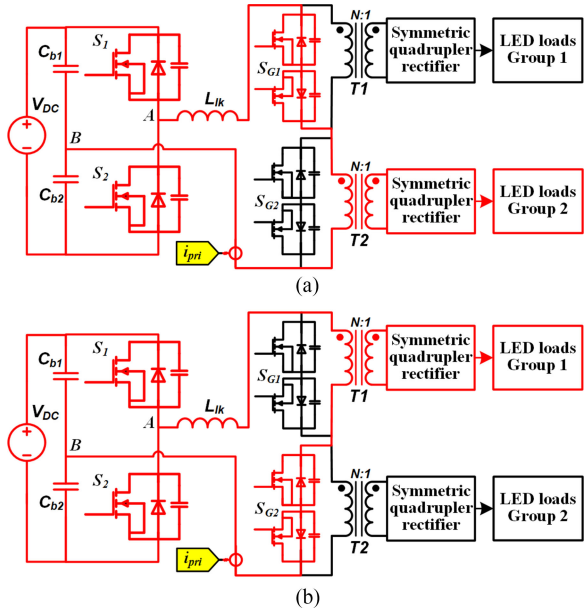

Fig. 2. Modes of operation for primary side shorting based on different states of the back-to-back switches S_{G1} and S_{G2} for LED Groups 1 and 2 (a) with S_{G1} ON and S_{G2} OFF (b) with S_{G1} OFF and S_{G2} ON.

and also meet the IEEE 1789 recommendation with 3 kHz dimming frequency. Also, during the selective dimming operation, the peak values of LED currents are controlled by using the peak current control method as proposed in [17]. The average values of LED currents are varied by the duty ratios of the back-to-back switches to perform selective dimming operations. The proposed topologies and modes of operation are presented in Section II. In Section III, the current control and theoretical loss analysis will be clearly illustrated and explained. Section IV presents the experimental and comparison results of the proposed topologies as well as their advantages of high efficiency in both full load and selective dimming operations.

II. Proposed Topologies and Modes of Operation

A. Proposed Topologies

The proposed topologies with selective dimming shown in Fig. 1 are based on an isolated dc–dc non-resonant converter [21] with equivalent dimming. Based on [21], the auxiliary back-to-back switches S_{G1} and S_{G2} are connected in parallel to the windings of transformers *T1* and *T2*, respectively, to achieve selective dimming for both LED Groups 1 and 2 in Fig. 1, where the back-to-back switches are connected from source to source while their drains are connected to the two separate ends of each respective winding, as shown in Fig. 1. The isolated gate drivers of S_{G1} and S_{G2} are powered by the housekeeping flyback converter with regulated voltage of 12 Vdc. In Fig. 1(a), the back-to-back switches are connected in parallel at primary side of transformer windings, and in Fig. 1(b), they are connected in parallel at secondary side of transformer windings.

Based on [17], the primary side peak current control method is used for the proposed topologies in Fig. 1. In this control method, the primary side current $i_{\rm pri}$ is sampled to control its peak value $I_{\rm pri,pk}$ at a fixed value, while the frequency $f_{\rm SW}$ of switches S_1 and S_2 is being varied. In this way, the peak value of LED currents is maintained during selective dimming with constant $I_{\rm pri,pk}$ and varied $f_{\rm SW}$. As a result, the average LED currents in Groups 1 and 2 are varied by the duty ratios of S_{G1} and S_{G2} at a given dimming frequency $f_{\rm dim}$ of 3 kHz.

B. Modes of Operation

For the proposed topologies shown in Fig. 1, the peak current control method is used to control $I_{\rm pri,pk}$ and LED peak currents. In Fig. 1, when both switches S_{G1} and S_{G2} are in OFF state, the dc–dc converter operates under normal condition as described in [21]. Fig. 2 shows the modes of operation for the method of primary side winding shorting in Fig. 1(a).

Fig. 2(a) illustrates the selective dimming operation when S_{G1} is in ON state, while S_{G2} is in OFF state. During this operation, $i_{\rm pri}$ is shorted through S_{G1}, therefore no current flows to transformer *T1* and the symmetric quadrupler rectifier at the secondary side of transformer *T1*. Consequently, all the LEDs in Group 1 are turned OFF, while the LEDs in Group 2 continue to operate normally. Fig. 2(b) illustrates the selective dimming operation when S_{G2} is in ON state, while S_{G1} is in OFF state. Comparably, during this operation, $i_{\rm pri}$ is shorted through S_{G2}, therefore

there is neither current flow to transformer *T2* nor through the quadrupler rectifier at the secondary side of transformer *T2*. As a result, all the LEDs in Group 2 are turned OFF, while the LEDs in Group 1 continue to operate normally.

When both LED groups are required to be turned OFF, instead of turning ON both switches $S_{\rm G1}$ and $S_{\rm G2}$, S_1 and S_2 will stop operating. This is to prevent short circuit and reduce power losses through the circuit when both $S_{\rm G1}$ and $S_{\rm G2}$ are in ON states. According to the above modes of operation, selective dimming of LED driver is operated through periodic switching between ON and OFF states of switches $S_{\rm G1}$ and $S_{\rm G2}$.

Similar modes of operation occur for the method of secondary side winding shorting in Fig. 1(b).

III. Current Control and Theoretical Loss Analysis of Proposed Converters

This section provides analysis of the proposed LED driver with the selective dimming function as well as developing the design for a prototype rated at 150 W. In this design, the LED driver prototype is supplied by input of 230 V rms and 60 Hz ac mains with 400 V intermediate dc bus voltage $V_{\rm DC}$. During LED conduction, the output voltage V_o and current I_o are 40 V and 450 mA, respectively, for each LED channel (12 LEDs in one channel [1]). The two LED groups of the proposed LED driver are applied with selective dimming of down to 5%, and its pulse-width modulation (PWM) dimming switching frequency of 3 kHz meets the IEEE 1789 recommendation. For this analysis, the methods in Fig. 1(a) and (b) are similar.

A. Analysis of Primary Side Peak Current Control Method

In [21], the constant frequency control method for switches S_1 and S_2 can transfer power through the transformers to drive the LEDs, however, it is unable to maintain the primary side peak current $I_{\rm pri,pk}$ at a fixed value during the transient change of LED loads. These instantaneous LED current pulses may resultantly exceed the rated current values, hence leading to overcurrent in LEDs. Consequently, such recurrent phenomenon will lead to electro-migration and eventually fast aging of LEDs [20].

As described in [17], $I_{\rm pri,pk}$ is kept constant under the peak current control method. In this way, there will not be any current pulses in the LEDs during their load transient states, unlike the constant frequency control method. Under the peak current control method, the switching frequency $f_{\rm SW}$ is varied based on $I_{\rm pri,pk}$ during the selective dimming operation.

For the peak current control method analyzed in [17], when the primary current $i_{\rm pri}$ reaches its peak, the switches S_1 and S_2 will change states. Therefore, because of the proportional relationship between $I_{\rm pri,pk}$ and LED peak current during the conducting state, both of them remain constant. According to [17], $f_{\rm SW}$ can be written as follows:

$$f_{\rm SW} = \frac{\frac{V_{\rm DC}^2}{4} - \left(|v_{\rm pri,T1}| + |v_{\rm pri,T2}|\right)^2}{2I_{\rm pri,pk}V_{\rm DC}L_{lk}} \quad (1)$$

$$v_{\rm pri,T1} = Nv_{\rm sec,T1} \quad (2)$$

$$v_{\rm pri,T2} = Nv_{\rm sec,T2}. \quad (3)$$

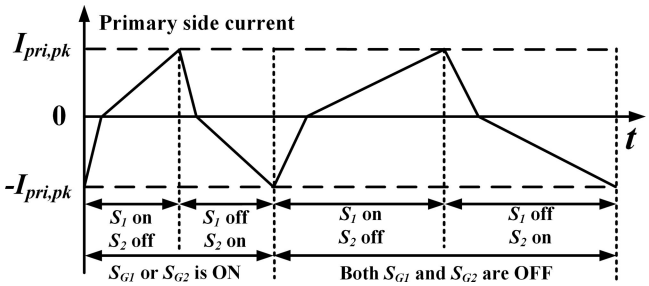

Fig. 3. Two separate conditions of switching frequency $f_{\rm SW}$ varied by different states of back-to-back switches $S_{\rm G1}$ and $S_{\rm G2}$ under peak current control.

According to principles of the quadrupler rectifier [22], $|v_{\rm sec,T1}|$ and $|v_{\rm sec,T2}|$ are equal to average output voltages of LED channels *CH1–CH4* $V_{\rm o(1-4)avg}$ in Group 1 and channels *CH5–CH8* $V_{\rm o(5-8)avg}$ in Group 2, respectively. Since N, $|v_{\rm sec,T1}|$, and $|v_{\rm sec,T2}|$ are constant, $|v_{\rm pri,T1}|$ and $|v_{\rm pri,T2}|$ are also constant based on (2) and (3).

Fig. 3 illustrates the two separate conditions of $f_{\rm SW}$ that varies according to different states of switches $S_{\rm G1}$ and $S_{\rm G2}$ under the peak current control. In Fig. 3, the magnitudes of $i_{\rm pri}$ are kept constant as defined by $\pm I_{\rm pri,pk}$. Ignoring the loss, the energy between the transformer primary side and secondary side should be equal. According to the above analysis, since $|v_{\rm pri,T1}|$ and $|v_{\rm pri,T2}|$ are constant, the energy equation between transformer primary side and secondary side can be given by the following equations:

$$|v_{\rm pri,T1}|\,|i_{\rm pri}|_{\rm avg} = |v_{\rm sec,T1}|\,|i_{\rm sec1}|_{\rm avg} = 4V_{o(1-4)\rm avg}I_o \quad (4)$$

$$|v_{\rm pri,T2}|\,|i_{\rm pri}|_{\rm avg} = |v_{\rm sec,}T2|\,|i_{\rm sec2}|_{\rm avg} = 4V_{o(5-8)\rm avg}I_o. \quad (5)$$

Since the rectified primary side current $|i_{\rm pri}|$ is shaped like a triangle, the relationship of its average value with $I_{\rm pri,pk}$ can be given by

$$|i_{\rm pri}|_{\rm avg} = \frac{1}{2}I_{\rm pri,pk}. \quad (6)$$

Based on (1)–(6), $f_{\rm SW}$ can be derived as follows:

$$f_{\rm SW} = N\frac{\frac{V_{\rm DC}^2}{4} - \left(NV_{o(1-4)\rm avg} + NV_{o(5-8)\rm avg}\right)^2}{16V_{\rm DC}L_{\rm lk}I_o}. \quad (7)$$

Hence, under the peak current control, $f_{\rm SW}$ is a function of I_o, $V_{\rm o(1\text{-}4)avg}$ and $V_{\rm o(5\text{-}8)avg}$.

B. Control of Primary Side Current and Currents in LEDs During Selective Dimming

Using peak current control method, the LED peak currents are controlled. To realize selective dimming operation, the average currents of both LED Groups 1 and 2 are controlled by the duty ratios of switches $S_{\rm G1}$ and $S_{\rm G2}$, respectively, at dimming frequency $f_{\rm dim}$. For the proposed topologies, the selective dimming operation is achieved by controlling the primary side peak current using switches S_1 and S_2 as well as controlling the average LED currents using back-to-back switches $S_{\rm G1}$ and $S_{\rm G2}$.

In this article, the dimming frequency $f_{\rm dim}$ is set at 3 kHz. This is because according to IEEE 1789 recommendation, the no-effect region of LED dimming frequency based on the PWM dimming should be more than 3 kHz [24]. With reference to the explanation in [17] and shown in (8), the average LED currents $I_{\rm avg,G1}$ and $I_{\rm avg,G2}$ of Groups 1 and 2, respectively, are varied according to the dimming percentages $D_{\%1}$ and $D_{\%2}$ of the respective LED Groups 1 and 2

$$I_{{\rm avg},Gi} = D_{\%i} I_o \tag{8}$$

where $i = 1$ or 2. As described in Section II-B, when both LED groups are required to be turned OFF, instead of turning ON both switches $S_{\rm G1}$ and $S_{\rm G2}$, switches S_1 and S_2 will stop operating. Thus, at $f_{\rm dim}$ of 3 kHz, the operating duty ratio $D_{\rm pri}$ of the primary side switches S_1 and S_2, dimming percentages $D_{\%1}$ and $D_{\%2}$ of the respective LED Groups 1 and 2, can be derived in the following equations:

$$D_{\rm pri} = \max\{D_{\%1}, D_{\%2}\} \tag{9}$$

$$D_{\%1} = D_{\rm pri} - D_{G1} \tag{10}$$

$$D_{\%2} = D_{\rm pri} - D_{\rm G2}. \tag{11}$$

C. Loss Analysis and Comparison of DC–DC Converter During Selective Dimming Operation Between Methods of Primary Side Shorting and Secondary Side Shorting

In this subsection, the loss of the proposed dc–dc converters with selective dimming is analyzed. Table I shows the theoretical analysis of loss for both the methods in Fig. 1. The parameters of $k_{\rm fe}$, A_e, l_m and the constant β can be determined from the datasheet and loss chart of the respective transformer core and series inductor core. The turn-ON loss of S_1 and S_2 is ignored due to complete zero voltage turning ON of MOSFETS as mentioned in [17].

Table II shows the theoretical analysis of power loss differences between methods of primary side shorting and secondary side shorting. For the switching loss of switches $S_{\rm G1}$ and $S_{\rm G2}$, they have no loss in no dimming state, have both turning-ON and turning-OFF losses in one-group dimming state, and have turning-OFF loss only in two-group dimming state since the voltage and current of transformer windings are zero when turning ON.

Table III shows the essential components of dc–dc converter with selective dimming. Based on Tables I–III, Fig. 4 shows the efficiency analysis of dc–dc converter with selective dimming for the method of primary side shorting. The dimming difference of percentage implies that the difference of dimming percentage of two LED groups, e.g., 50% output of Group 1 and 30% output of Group 2 for total 40% output with 20% dimming difference. One LED group maintaining full load with another group dimming is named as one group dimming. For any dimming conditions, 0.44 W auxiliary power consumption for micro-controller and signal circuits is considered.

According to (9)–(11), if $D_{\%1} > D_{\%2}$, $D_{\rm pri} = D_{\%1}$ and $\Delta D_{\%} = D_{\%1} - D_{\%2}$. For same power level, $(D_{\%1} + D_{\%2})$ is constant. Hence, under this condition, as $\Delta D_{\%}$ increases, $D_{\%1}$ increases while $D_{\%2}$ decreases, and hence $D_{\rm pri}$ increases. Since most of the power losses are directly proportional to $D_{\rm pri}$ based on Tables I and II, the total power losses increase with increased $D_{\rm pri}$. Hence, as the dimming difference $\Delta D_{\%}$ of two LED groups increases, the efficiency will drop under same output power as shown in Fig. 4. It is same for the condition of $D_{\%2} > D_{\%1}$. For one group dimming, the dimming difference $\Delta D_{\%}$ is largest under same output power conditions. Hence, the efficiency under one group dimming is lowest, as shown in Fig. 4. The loss and efficiency analysis results are similar for the method of secondary side shorting.

TABLE I
THEORETICAL LOSS ANALYSIS OF THE PROPOSED TWO TOPOLOGIES WITH SELECTIVE DIMMING

Total loss	Description	Equations	
MOSFET S_1 and S_2	Conduction loss $P_{\rm cM}$	$2\left(\frac{I_{\rm pri,pk}}{\sqrt{6}}\right)^2 R_{\rm DSon,pri} D_{pri}$	(12)
	Switching loss $P_{\rm swM}$	$2\times\frac{1}{2} V_{DC} I_{\rm pri,pk} t_{\rm f,pri} \left(\begin{array}{l} f_{\rm SW,no}\left(D_{pri} - \lvert D_{\%1} - D_{\%2}\rvert\right) \\ + f_{\rm SW,one}\lvert D_{\%1} - D_{\%2}\rvert \end{array}\right)$	(13)
Diode D_1-D_8	Conduction loss $P_{\rm cD}$	$4V_{\rm F}\frac{I_{\rm pri,pk} N}{8}\left(D_{\%1} + D_{\%2}\right)$	(14)
Transformer $T1$ and $T2$	Core loss $P_{{\rm core},T}$	$k_{fe} A_e l_m \left(\begin{array}{l} \left(\Delta B_{no}\right)^{\beta}\times 2\left(D_{pri} - \lvert D_{\%1} - D_{\%2}\rvert\right) \\ + \left(\Delta B_{one}\right)^{\beta}\lvert D_{\%1} - D_{\%2}\rvert \end{array}\right)$	(15)
Series Inductor	Core loss $P_{{\rm core},L}$	$k_{fe} A_e l_m \left(\begin{array}{l} \left(\Delta B_{no}\right)^{\beta}\left(D_{pri} - \lvert D_{\%1} - D_{\%2}\rvert\right) \\ + \left(\Delta B_{one}\right)^{\beta}\lvert D_{\%1} - D_{\%2}\rvert \end{array}\right)$	(16)
	Copper loss $P_{{\rm Cu},L}$	$\left(\frac{I_{\rm pri,pk}}{\sqrt{3}}\right)^2 R_{Llk} D_{pri}$	(17)

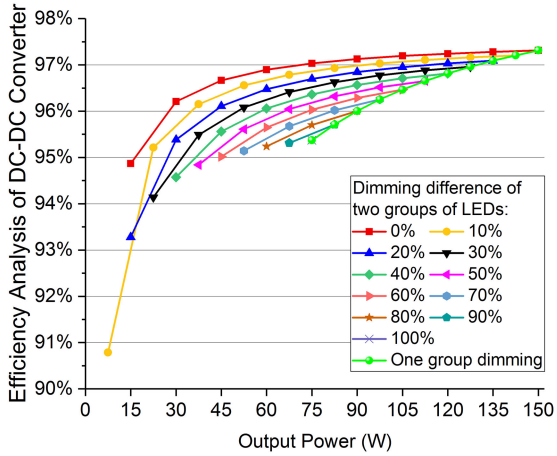

Fig. 4. Efficiency analysis of the dc-dc converter with selective dimming operation at dimming differences from 0% to 100% with 10% increments under the method of primary side shorting.

TABLE II
THEORETICAL ANALYSIS OF POWER LOSS DIFFERENCES BETWEEN METHODS OF PRIMARY SIDE SHORTING AND SECONDARY SIDE SHORTING

Total loss	Description	Equations	
		Primary Side Shorting	Secondary Side Shorting
Transformer $T1$ and $T2$	Copper loss $P_{\mathrm{Cu},T}$	$\left(\frac{I_{pri,pk}}{\sqrt{3}}\right)^2\left(R_{pri}+N^2R_{sec}\right)(D_{\%1}+D_{\%2})=\alpha_1\times(D_{\%1}+D_{\%2})$ (18)	$2\left(\frac{I_{\mathrm{pri,pk}}}{\sqrt{3}}\right)^2\left(R_{\mathrm{pri}}+N^2R_{\mathrm{sec}}\right)D_{pri}=\alpha_2\times 2D_{pri}$ (19)
MOSFET S_{G1} and S_{G2}	Conduction loss P_{cSG}	$\left(\frac{I_{pri,pk}}{\sqrt{3}}\right)^2 2R^{pri}_{DSon,SG}\left(2D_{pri}-D_{\%1}-D_{\%2}\right)=\beta_1\times\left(2D_{pri}-D_{\%1}-D_{\%2}\right)$ (20)	$\left(\frac{I_{pri,pk}N}{\sqrt{3}}\right)^2 2R^{sec}_{DSon,SG}\left(2D_{pri}-D_{\%1}-D_{\%2}\right)=\beta_2\times\left(2D_{pri}-D_{\%1}-D_{\%2}\right)$ (21)
	Switching loss P_{swSG}	$\frac{1}{2}\left(C^{pri}_{OSS}N^2V_o^2+NV_oI_{pri,pk}t^{pri}_{r,SG}+NV_oI_{pri,pk}t^{pri}_{f,SG}\right)f_{dim}=\gamma_1$ (22)	$\frac{1}{2}\left(C^{sec}_{OSS}V_o^2+V_oI_{pri,pk}Nt^{sec}_{r,SG}+V_oI_{pri,pk}Nt^{sec}_{f,SG}\right)f_{dim}=\gamma_2$ (23)

TABLE III
ESSENTIAL COMPONENTS OF TWO PROPOSED DC–DC CONVERTERS WITH SELECTIVE DIMMING

Symbol	Description	Parameter
S_1,S_2	Power MOSFETs	IPP65R190C7 (650 V)
S_{G1},S_{G2}	Power MOSFETs	SIR690DP-TI-TE3 (200 V) (for primary side shorting) SIR668DP-TI-RE3 (100 V) (for secondary side shorting)
$T1$,$T2$	Transformer	PQ-2625, 3C95, Ferroxcube. Primary: 29Ts, 105/42 litz wire; Secondary: 16Ts, 85/39 litz wire; Magnetizing inductance: 5.7 mH (120 kHz) on primary side winding; Leakage inductance: 12 μH reflected on primary side.
D_1-D_8	Output diodes	TSP15H120S S1G
C_{b1},C_{b2}	Intermediate capacitor	2.2 μF, 250V ECQ-E2225KF
C_{blk1},C_{blk2}	Blocking capacitor	2.2 μF, 100V CL32B225KCJSNNE
C_1-C_2, C_7-C_8	Quadrupler capacitor	2.2 μF, 100V CL32B225KCJSNNE
C_3-C_6, C_9-C_{12}	Output capacitor	2 × 4.7 μF, 80V GRM32ER71K475KE14L

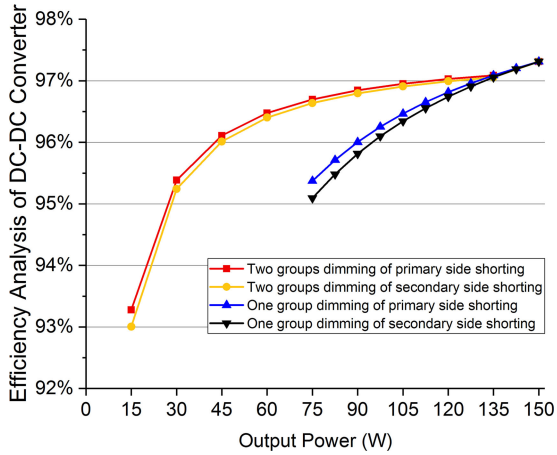

Fig. 5. Efficiency comparison of dc-dc converters with selective dimming operation at one-group dimming and two-group dimming of 20% dimming difference under methods of primary side shorting and secondary side shorting.

The loss comparison of two proposed methods is defined as follows:

$$\begin{aligned}\Delta P_{\mathrm{loss}} &= \Delta P_{\mathrm{Cu},T}+\Delta P_{\mathrm{cSG}}+\Delta P_{\mathrm{swSG}}\\ &= \left(P^{\mathrm{sec}}_{\mathrm{Cu},T}-P^{\mathrm{pri}}_{\mathrm{Cu},T}\right)+\left(P^{\mathrm{sec}}_{\mathrm{cSG}}-P^{\mathrm{pri}}_{\mathrm{cSG}}\right)\\ &\quad+\left(P^{\mathrm{sec}}_{\mathrm{swSG}}-P^{\mathrm{pri}}_{\mathrm{swSG}}\right).\end{aligned}\tag{24}$$

Based on Tables II and III, the coefficients can be calculated that $\alpha_1=\alpha_2=0.2354$, $\beta_1=0.09333$, $\beta_2=0.04147$, $\gamma_1=0.00680$, and $\gamma_2=0.00791$. Since $\gamma_1<\gamma_2$, $\Delta P_{\mathrm{swSG}}=\gamma_2-\gamma_1$ is always greater than zero under same dimming conditions of two methods. ΔP_{swSG} is constant, hence ΔP_{loss} can be expressed as follows:

$$\Delta P_{\mathrm{loss}}=(\alpha_2+\beta_2-\beta_1)\,(2D_{\mathrm{pri}}-D_{\%1}-D_{\%2})+\Delta P_{\mathrm{swSG}}.\tag{25}$$

From (25), $(\alpha_2+\beta_2-\beta_1)=0.18354>0$. Hence, $\Delta P_{\mathrm{loss}}>0$ for all values of D_{pri}, $D_{\%1}$, and $D_{\%2}$. As a result, the power loss for the method of secondary side shorting is always greater than the primary side shorting under the same dimming condition.

According to (25), ΔP_{loss} is proportional to $(2D_{\mathrm{pri}}-D_{\%1}-D_{\%2})$. From (9), if $D_{\%1}>D_{\%2}$, $D_{\mathrm{pri}}=D_{\%1}$. Hence, ΔP_{loss} is proportional to $\Delta D_{\%}=D_{\%1}-D_{\%2}$. For the same total output power level, $(D_{\%1}+D_{\%2})$ is constant. Hence, as $\Delta D_{\%}$ increases, $D_{\%1}$ increases and $D_{\%2}$ decreases, which leads to increased ΔP_{loss}.

According to the above analysis, Fig. 5 shows the efficiency comparison of the two proposed methods at one-group dimming and two-group dimming of 20% dimming difference. For two-group dimming of 20% dimming difference, although the efficiency of primary side shorting is a bit higher than secondary side shorting as analyzed in (25), the difference in efficiency between the two methods is not significant, as shown in Fig. 5. However, for the one-group dimming, where $D_{\%1}=1$, $\Delta D_{\%}$ increases with reduced $D_{\%2}$. Hence, ΔP_{loss} increases with the reduced output power. As a result, the difference in efficiency between two methods becomes larger with reduced power at one-group dimming operation, as shown in Fig. 5.

According to the values of coefficients, α_1 and α_2 are several times larger than β_1 and β_2, and β_1 and β_2 are much larger than γ_1 and γ_2. Hence, the main loss difference of these two methods is the transformer copper loss according to Table II. This shows

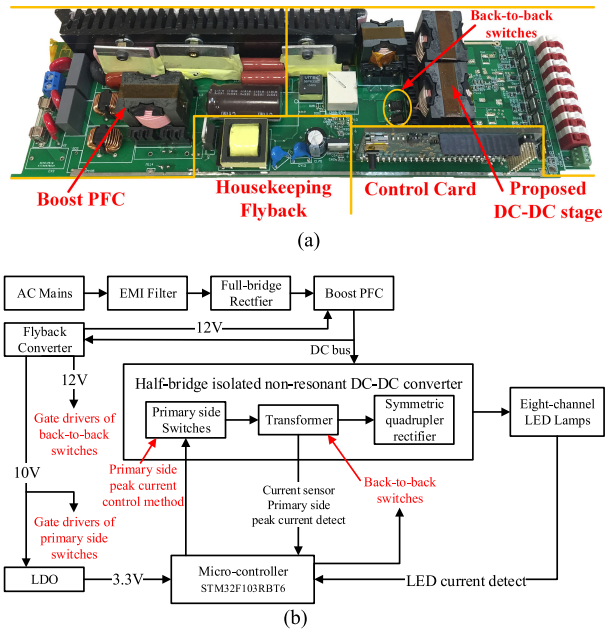

Fig. 6. Proposed two-stage multichannel selective dimming (3 kHz) LED driver with the method of primary side shorting. (a) Prototype (27 cm × 7 cm). (b) Overall block diagram.

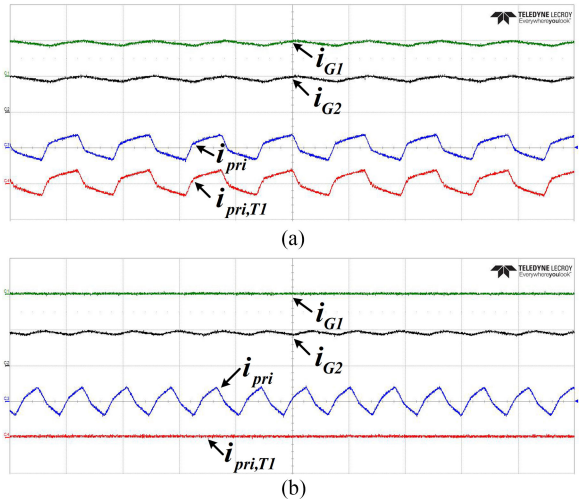

Fig. 7. Steady-state waveforms of LED currents i_{G1} and i_{G2} in Groups 1 and 2 respectively, primary side current i_{pri}, and current of primary side winding of transformer *T1* $i_{pri,T1}$ of proposed LED driver under peak current control method with primary side shorting. (a) Both Groups 1 and 2 at full load state (b) in Group 1 no load state and Group 2 full load state (i_{G1} and i_{G2}: 500 mA/div, i_{pri} and $i_{pri,T1}$: 5 A/div, *t*: 10 μs/div).

the advantage of the method of primary side shorting compared to secondary side shorting.

IV. Experimental Results

Fig. 6(a) illustrates the proposed two-stage multichannel selective dimming (3 kHz) LED driver prototype with the method of primary side shorting rated at output power of 150 W. Fig. 6(b) shows the overall block diagram of this LED driver. The LED driver is supplied by input of 230 V rms and 60 Hz ac mains. The first stage of this prototype is the well-known full-bridge boost power factor correction (PFC) converter controlled by IC TI UCC28180D with output dc bus voltage V_{DC} of 400 V. Under input of V_{DC}, the housekeeping flyback converter generates primary side dc output at 12 V to supply the PFC control IC. The flyback converter also generates secondary side dc output at 10 V to supply the gate drivers of switches S_1 and S_2. To generate a 3.3 V output for the signal circuit and micro-controller power supply, an low dropout regulator (LDO) with secondary side dc voltage input is used. Two auxiliary windings from the flyback transformer with half-bridge rectifiers are used to power two isolated gate drivers of switches S_{G1} and S_{G2} at 12 V, and hence it avoids using the auxiliary isolated dc–dc converters. The second stage of the prototype is the proposed isolated dc–dc non-resonant converter with selective dimming by the method of primary side shorting with V_{DC} input, as shown in Fig. 1(a). The micro-controller STM32F103RBT6 is used to perform peak current control and selective dimming operation. The prototype with the method of secondary side shorting is similar compared to primary side shorting. For the method of secondary side shorting, the switches S_{G1} and S_{G2} are removed from primary side to secondary side of transformer windings.

Figs. 7–14 are based on the method of primary side shorting. The experimental results of the method of secondary side shorting are similar to the method of primary side shorting.

Fig. 7 shows the waveforms of LED currents i_{G1} and i_{G2} of Groups 1 and 2, respectively, primary side current i_{pri}, and current of primary side winding of transformer *T1* $i_{pri,T1}$ at steady state of the proposed LED driver using peak current control with the method of primary side shorting. Fig. 7(a) shows the LED currents under no dimming state (full load at 450 mA) at switching frequency f_{SW} of 76 kHz which is equal to that of i_{pri}. $i_{pri,T1}$ follows the dimming condition of LED Group 1, and hence it is equal to i_{pri} at full load of Group 1 as shown in Fig. 7(a). Fig. 7(b) shows the Group 1 LED current i_{G1} at no load and Group 2 LED current i_{G2} at full load at f_{SW} of 128 kHz. In Fig. 7(b), $i_{pri,T1}$ is zero since Group 1 is at no load. Under the peak current control, the peak values of i_{G1}, i_{G2}, i_{pri}, and $i_{pri,T1}$ are kept constant during their ON states as shown in Fig. 7.

Figs. 8 and 9 show the waveforms of i_{G1}, i_{G2}, i_{pri}, and $i_{pri,T1}$ under peak current control with the method of primary side shorting for one-group and two-group selective dimming operations, respectively. The average currents of respective dimming groups of LEDs are kept at corresponding values, and their peak values are controlled during the ON states.

According to Figs. 7–9, the higher value of either i_{G1} or i_{G2} follows the operation duty ratio of i_{pri}, which is the same as the analysis in (9)–(11), and the average value of i_{G1} follows that of operation duty ratio of $i_{pri,T1}$, as analyzed in Fig. 2. Hence, when LED Group 1 undergoes full dimming state (no load), $i_{pri,T1}$ goes to zero current (no current flowing).

Fig. 10 shows the waveforms of i_{G1}, i_{G2}, i_{pri}, and $i_{pri,T1}$ under the constant frequency control with the method of primary side shorting for selective dimming. In Fig. 10(a), the average and peak values of LED current in Group 2 increase by 20% and

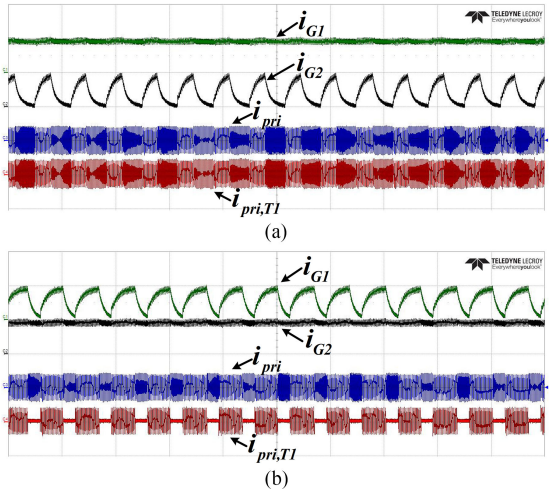

Fig. 8. Selective dimming waveforms of i_{G1}, i_{G2}, i_{pri}, and $i_{pri,T1}$ of the proposed LED driver under peak current control method with primary side shorting. (a) i_{G1} at full load and i_{G2} at 200 mA average. (b) i_{G1} at 300 mA average and i_{G2} at full load (i_{G1} and i_{G2}: 500 mA/div, i_{pri} and $i_{pri,T1}$: 5 A/div, t: 500 μs/div).

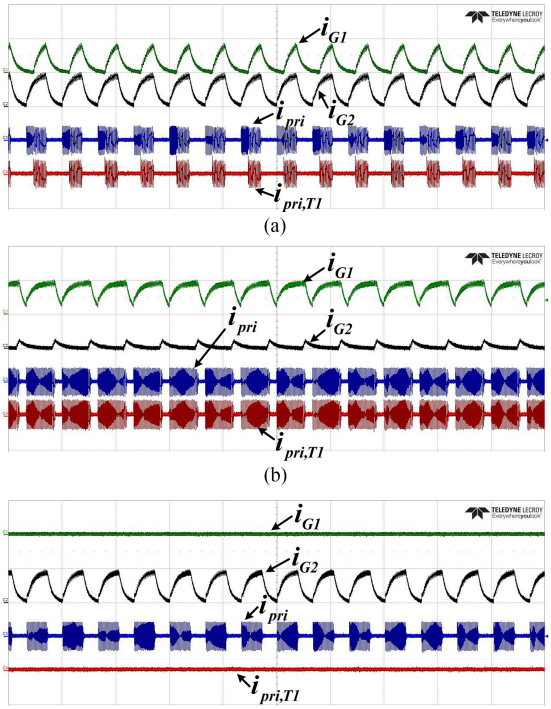

Fig. 9. Selective dimming waveforms of i_{G1}, i_{G2}, i_{pri}, and $i_{pri,T1}$ of proposed LED driver under peak current control method with primary side shorting. (a) i_{G1} at 150 mA average and i_{G2} at 250 mA average. (b) i_{G1} at 350 mA average and i_{G2} at 25 mA average. (c) i_{G1} at no load and i_{G2} at 250 mA average (i_{G1} and i_{G2}: 500 mA/div, i_{pri} and $i_{pri,T1}$: 5 A/div, t: 500 μs/div).

50%, respectively, during the dimming operation, as compared to the same dimming conditions in Fig. 8(b) under peak current control. In Fig. 10(b), under two-group dimming operation, although the average LED currents of both Groups 1 and 2 are controlled at corresponding values, the peak value of LED

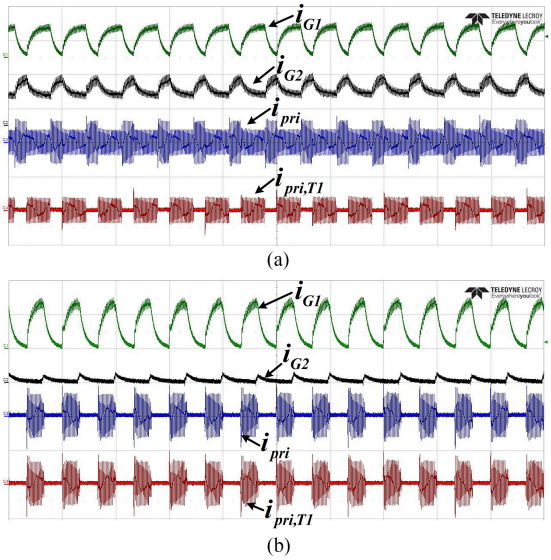

Fig. 10. Selective dimming waveforms of i_{G1}, i_{G2}, i_{pri}, and $i_{pri,T1}$ of the proposed LED driver under constant frequency control method with primary side shorting. (a) i_{G1} at 300 mA average and i_{G2} at full load. (b) i_{G1} at 350 mA average and i_{G2} at 25 mA average (i_{G1} and i_{G2}: 500 mA/div, i_{pri} and $i_{pri,T1}$: 5 A/div, t: 500 μs/div).

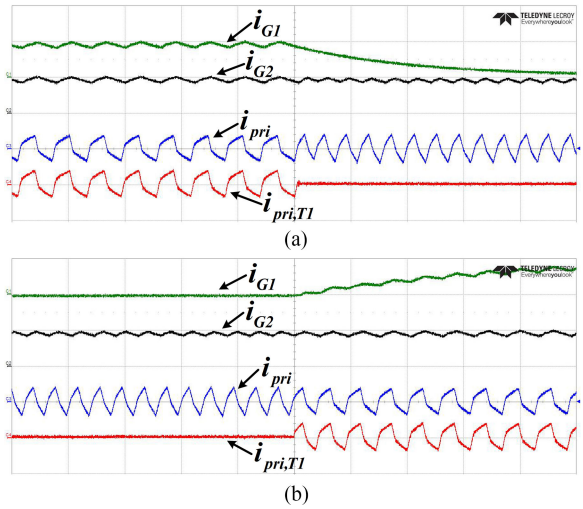

Fig. 11. Transient states of i_{G1}, i_{G2}, i_{pri} and $i_{pri,T1}$ of proposed LED driver under peak current control method with primary side shorting. (a) Group 1 from ON to OFF state and Group 2 at full load. (b) Group 1 from OFF to ON state and Group 2 at full load (i_{G1} and i_{G2}: 500 mA/div, i_{pri} and $i_{pri,T1}$: 5 A/div, t: 20 μs/div).

current for Group 1 increases by a significant 48% as compared to that of Fig. 9(b) under peak current control. The significant increase in peak values of LED currents will exceed the threshold values of LEDs and in turn reduce their lifetimes [20]. This shows the advantage of the peak current control method.

Figs. 11–13 show the transient states of i_{G1}, i_{G2}, i_{pri}, and $i_{pri,T1}$ under peak current control with the method of primary side shorting for selective dimming. In Fig. 11, LEDs in Group 2 are set at full load throughout, while LEDs in Group 1 undergo transient states from ON to OFF and vice-versa. In Fig. 11(a),

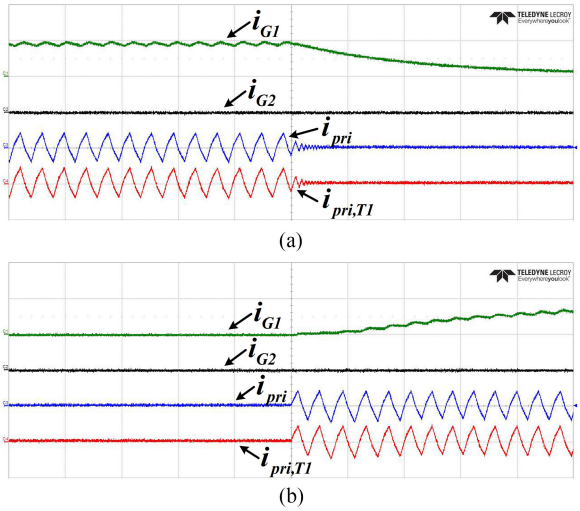

Fig. 12. Transient states of i_{G1}, i_{G2}, i_{pri}, and $i_{pri,T1}$ of the proposed LED driver using peak current control method with primary side shorting. (a) Group 1 from ON to OFF state and Group 2 at no load. (b) Group 1 from OFF to ON state and Group 2 at no load (i_{G1} and i_{G2}: 500 mA/div, i_{pri} and $i_{pri,T1}$: 5 A/div, t: 20 μs/div).

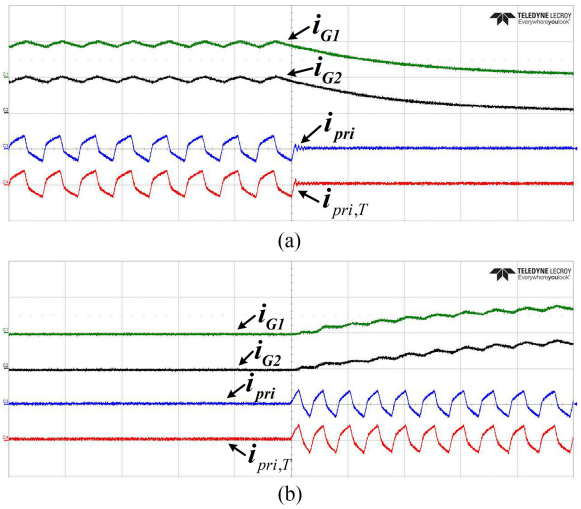

Fig. 13. Transient states of i_{G1}, i_{G2}, i_{pri}, and $i_{pri,T1}$ of the proposed LED driver under peak current control method with primary side shorting. (a) Both Groups 1 and 2 from full load to no load. (b) Both Groups 1 and 2 from no load to full load (i_{G1} and i_{G2}: 500 mA/div, i_{pri} and $i_{pri,T1}$: 5 A/div, t: 20 μs/div).

during the transient state when LEDs in Group 1 changes from ON to OFF state, the switching frequency f_{SW} of switches S_1 and S_2 increases. Vice-versa, in Fig. 11(b), f_{SW} decreases during the transient state when LEDs in Group 1 changes from OFF to ON state. Fig. 12 shows LEDs in Group 2 are kept at no load throughout while LEDs in Group 1 undergo transient states from ON to OFF and vice-versa. In Fig. 12, the switches S_1 and S_2 operate at high switching frequency (128 kHz) under LED conducting condition. Fig. 13 shows both groups of LEDs undergo transient states from ON to OFF and vice-versa at the same time. In Fig. 13, the switches S_1 and S_2 operate at low switching frequency (76 kHz) under LED conducting condition.

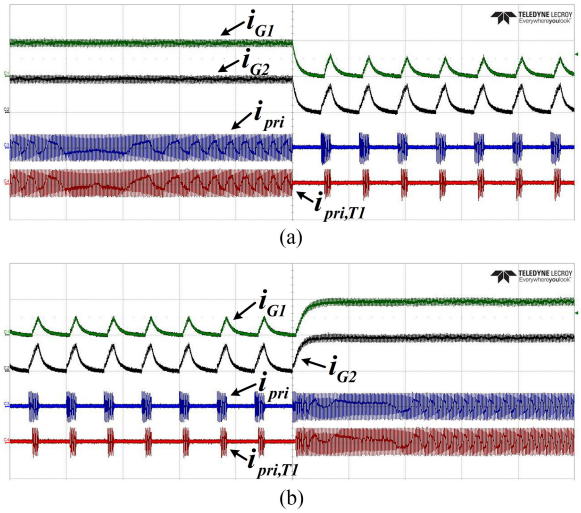

Fig. 14. Dynamic performance of i_{G1}, i_{G2}, i_{pri}, and $i_{pri,T1}$ of the proposed LED driver under peak current control method with primary side shorting (a) from both groups at full load to Group 1 at 10% and Group 2 at 20% output power and (b) from Group 1 at 10% and Group 2 at 20% output power to both groups at full load (i_{G1} and i_{G2}: 500 mA/div, i_{pri} and $i_{pri,T1}$: 5 A/div, t: 500 μs/div).

According to Figs. 11–13, the peak current control method performs well for transient of dimming for both LED groups.

Fig. 14 shows dynamic performances of i_{G1}, i_{G2}, i_{pri}, and $i_{pri,T1}$ under peak current control with the method of primary side shorting. Fig. 14(a) shows dynamic transient states of both Groups 1 and 2 from full load to respective 10% and 20% output power. Fig. 14(b) shows dynamic transient states of Groups 1 and 2 from respective 10% and 20% output power to full load.

Fig. 15(a) shows the efficiency of the proposed dc–dc part of LED driver with the method of primary side shorting at dimming frequency of 3 kHz. The efficiencies are based on the dimming difference between two groups of LEDs from 0% to 100% at 10% increments. Similar to the analysis in Fig. 4, under same output power, the efficiency decreases as the dimming difference between the two groups of LEDs increases.

Fig. 15(b) shows the comparison of dimming efficiency of the proposed dc–dc part of LED drivers under one-group dimming and two-group dimming (20% dimming difference) operations between methods of primary side shorting and secondary side shorting. For both dimming operations, the method of primary side shorting has higher efficiency than secondary side shorting, which is the same as analyzed in Section III-C. For one-group dimming condition, the difference of efficiency between the primary side shorting and secondary side shorting increases with reduced output power, as shown in Fig. 15(b), which is same as analyzed in Fig. 5.

In Fig. 15(c), the dimming efficiencies of the dc–dc part of LED drivers among the proposed primary side shorting topology, secondary side shorting topology, and LED drivers in [11], [14], [15], [17] are compared. The dimming frequency for methods of primary side shorting and secondary side shorting is 3 kHz, and while the same is only 250 Hz in [17]. For the same output power, the two proposed methods of selective dimming

TABLE IV
COMPARISON OF THE EXISTING LED DRIVERS FOR *N* GROUPS OF LEDS SELECTIVE DIMMING

Paper	Topology for isolation	No. of LED channels	Dimming method	PWM dimming frequency	DC bus input voltage	Output power	Maximum efficiency at input ac rms voltage		
							Whole system	Isolated DC-DC & dimming circuit	Input ac rms voltage
[9]	Flyback	*N*	PWM	240 Hz	/	20 W	/	/	110/230 V
[10]	Resonant	*2N*	AM	/	48 V	20 W	/	93.4%	/
[11]	Resonant	*N*	AM/PWM	300 Hz	400 V	60 W	/	85.5%	/
[12]	Forward	*N*	AM/PWM	200 Hz	20-30 V	16.5 W	/	88%	/
[13]	Forward	*N*	PWM	60 Hz	400 V	30 W	/	/	/
[14]	Forward	*N*	AM	/	48 V	54.4 W	/	86%	/
[15]	Non-resonant	*N*	AM	/	380 V	50 W	/	90.5%	/
[16]	Resonant	*N*	AM/PWM	200 Hz	400 V	100 W	87.5%	/	240 V
[17]	Non-resonant	*2N*	AM/PWM	250 Hz	400 V	150 W	94.3%	97.3%	230 V
Proposed primary	Non-resonant	*4N*	AM/PWM	3 kHz	400 V	150 W	94.3%	97.3%	230 V
Proposed secondary	Non-resonant	*4N*	AM/PWM	3 kHz	400 V	150 W	94.3%	97.3%	230 V

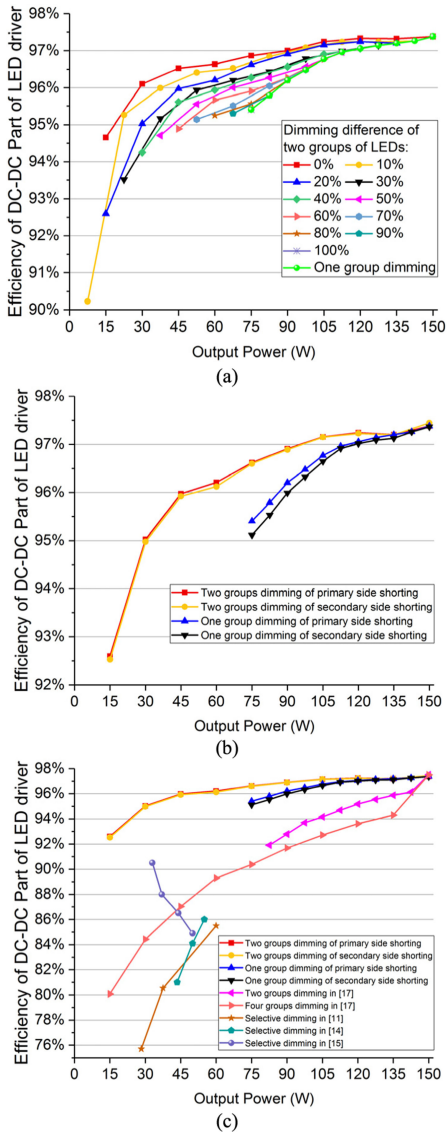

Fig. 15. (a) Dimming efficiency of proposed dc-dc part of LED driver based on method of primary side shorting at dimming frequency of 3 kHz. (b) Comparison of dimming efficiency of proposed dc–dc part of LED drivers between primary side shorting and secondary side shorting topologies. (c) Comparison of dimming efficiency of dc–dc part of LED drivers among proposed primary side shorting topology, secondary side shorting topology and LED drivers in [11], [14], [15], and [17].

have higher efficiencies than the LED drivers in [11], [14], [15], and [17].

The two proposed methods in this article have the advantage of higher efficiencies during selective dimming since it avoids the issue in [17] that the energy from output capacitors of LED channels is wasted during each PWM dimming switching cycle, and the loss will be higher with increased dimming frequency, output capacitance, and number of dimming groups as shown in the following equation:

$$P_{\text{auxLoss}} = m\frac{1}{2}C_o V_G^2 f_{\text{dim}}. \tag{26}$$

In [17], V_G is typically 80 V, and f_{dim} is 250 Hz. The summary of comparison among the two proposed methods and the existing LED drivers for selective dimming [PWM or amplitude modulation (AM) dimming] is shown in Table IV. Based on Table IV, most of the previous methods including their own work would implement selective dimming at frequencies less than 500 Hz and fail to meet the IEEE 1789 dimming recommendation which requires PWM dimming frequency to be at least 3 kHz for working in the no-effect region. The AM-based dimming methods for previous work have lower efficiency with variable inductor control method due to higher loss of variable bulky inductors for each channel of LEDs in [14] and [15]. The two proposed methods in this article use the methods of shorting primary side or secondary side windings of transformers for selective dimming, so that the dimming frequency is independent on the losses incurred. Therefore, the proposed methods in this article achieve the efficiency improvement of selective dimming for multichannel LED driver and meet IEEE 1789 recommendation for LED dimming.

V. CONCLUSION

In this article, two selective dimming methods have been proposed to improve the dimming efficiency of the two-stage multichannel LED driver. The new solutions utilize back-to-back switches connected in parallel with each respective primary side or secondary side transformer windings, to prevent power loss caused by output capacitor energy wasted through dimming switches at every dimming period in [17], and also meet the IEEE 1789 recommendation with 3 kHz dimming frequency. During selective dimming, the LED peak currents are controlled under

peak current control method. As such, the average currents of each respective LED group are varied according to duty ratios of back-to-back switches. The proposed topologies, modes of operation, detailed theoretical analyses have been covered in this article. A 150 W LED driver prototype and a non-DSP microcontroller are implemented to verify the theoretical analysis. The experimental results validate the improved efficiency in the dimming operation of the proposed topologies. The comparisons between the two proposed methods and the converters reported previously have been presented.

REFERENCES

[1] Cree LED datasheet. 2018. [Online]. Available: http://www.cree.com/led-components/media/documents/ds-XBD.pdf

[2] G.-S. Seo, H.-J. Kim, K.-C. Lee, S.-J. Choi, and B.-H. Cho, "DC-level dimmable LED driver with primary side on-time control for dc distribution," *IEEE J. Emerg. Sel. Topics Power Electron.*, vol. 3, no. 3, pp. 624–632, Sep. 2015.

[3] S. Li, Y. Guo, S.-C. Tan, and S. R. Hui, "An off-line single-inductor multiple-output LED driver with high dimming precision and full dimming range," *IEEE Trans. Power Electron.*, vol. 32, no. 6, pp. 4716–4727, Jun. 2017.

[4] M. Tahan and T. Hu, "Multiple string LED driver with flexible and high-performance PWM dimming control," *IEEE Trans. Power Electron.*, vol. 32, no. 12, pp. 9293–9306, Dec. 2017.

[5] Z. Dong, K. T. Chi, and S. R. Hui, "Current-source-mode single-inductor multiple-output LED driver with single closed-loop control achieving independent dimming function," *IEEE J. Emerg. Sel. Topics Power Electron.*, vol. 6, no. 3, pp. 1198–1209, Sep. 2018.

[6] Y. Guo, S. Li, A. T. Lee, S.-C. Tan, C. K. Lee, and S. R. Hui, "Single-stage AC/DC single-inductor multiple-output LED drivers," *IEEE Trans. Power Electron.*, vol. 31, no. 8, pp. 5837–5850, Aug. 2016.

[7] A. T. Lee, J. K. Sin, and P. C. Chan, "Scalability of quasi-hysteretic FSM-based digitally controlled single-inductor dual-string buck LED driver to multiple strings," *IEEE Trans. Power Electron.*, vol. 29, no. 1, pp. 501–513, Jan. 2014.

[8] H. Wu, S.-C. Wong, K. T. Chi, and Q. Chen, "A PFC single-coupled-inductor multiple-output LED driver without electrolytic capacitor," *IEEE Trans. Power Electron.*, vol. 34, no. 2, pp. 1709–1725, Feb. 2019.

[9] T. Ching, "Modular dimmable light-emitting-diode driver for general illumination applications," in *Proc. 23rd Canadian Conf. Elect. Comput. Eng.*, 2010, pp. 1–4.

[10] J. Liu, W. Sun, and J. Zeng, "Precise current sharing control for multi-channel LED driver based on switch-controlled capacitor," *IET Power Electron.*, vol. 10, no. 3, pp. 357–367, 2017.

[11] C. Wong, K. Loo, H. H.-C. Iu, Y. Lai, M. H. Chow, and K. T. Chi, "Independent control of multicolor-multistring LED lighting systems with fully switched-capacitor-controlled *LCC* resonant network," *IEEE Trans. Power Electron.*, vol. 33, no. 5, pp. 4293–4305, May 2018.

[12] W. Chen and S. Hui, "A dimmable light-emitting diode (LED) driver with mag-amp postregulators for multistring applications," *IEEE Trans. Power Electron.*, vol. 26, no. 6, pp. 1714–1722, Jun. 2011.

[13] C.-C. Chen, C.-Y. Wu, and T.-F. Wu, "Fast transition current-type burst-mode dimming control for the LED back-light driving system of LCD TV," in *Proc. 37th IEEE Power Electron. Spec. Conf*, 2006, pp. 1–7.

[14] R. A. Pinto, J. M. Alonso, M. S. Perdigão, M. F. da Silva, and R. N. do Prado, "A new technique to equalize branch currents in multiarray LED lamps based on variable inductors," *IEEE Trans. Ind. Appl.*, vol. 52, no. 1, pp. 521–530, Jan./Feb. 2016.

[15] J. M. Alonso, M. S. Perdigão, M. A. Dalla Costa, G. Martínez, and R. Osorio, "Analysis and experiments on a single-inductor half-bridge LED driver with magnetic control," *IEEE Trans. Power Electron.*, vol. 32, no. 12, pp. 9179–9190, Dec. 2017.

[16] X. Qu, S.-C. Wong, and K. T. Chi, "Noncascading structure for electronic ballast design for multiple LED lamps with independent brightness control," *IEEE Trans. Power Electron.*, vol. 25, no. 2, pp. 331–340, Feb. 2010.

[17] C. Ye, P. Das, and S. K. Sahoo, "Peak current control of multichannel LED driver with selective dimming," *IEEE Trans. Ind. Electron.*, vol. 66, no. 5, pp. 3446–3457, May 2019.

[18] Y. Cikai, P. Das, S. S. Kumar, and M. Pahlevaninezhad, "A multi-channel LED driver with selective dimming," in *Proc. IEEE Appl. Power Electron. Conf. Expo.*, 2018, pp. 2221–2226.

[19] "UL 8750 standard for light emitting diode (LED) equipment for use in lighting products." 2015. [Online]. Available: https://standardscatalog.ul.com/standards/en/standard_8750_2

[20] "Pulsed over-current driving of cree xlamp LEDs: Information and cautions." 2016. [Online]. Available: http://www.cree.com/led-components/media/documents/XLampPulsedCurrent.pdf

[21] R. Kathiresan, P. Das, T. Reindl, and S. K. Panda, "Novel high-power nonresonant multichannel LED driver," *IEEE Trans. Ind. Electron.*, vol. 64, no. 7, pp. 5851–5864, Jul. 2017.

[22] Y. Zhao, X. Xiang, W. Li, X. He, and C. Xia, "Advanced symmetrical voltage quadrupler rectifiers for high step-up and high output-voltage converters," *IEEE Trans. Power Electron.*, vol. 28, no. 4, pp. 1622–1631, Apr. 2013.

[23] T. LaBella, W. Yu, J. Lai, M. Senesky, and D. Anderson, "A bidirectional-switch-based wide-input range high-efficiency isolated resonant converter for photovoltaic applications," *IEEE Trans. Power Electron.*, vol. 29, no. 7, pp. 3473–3484, Jul. 2014.

[24] C. Ye, P. Das, and S. K. Sahoo, "Peak current control based power ripple decoupling of AC-DC multi-channel LED driver," *IEEE Trans. Ind. Electron.*, vol. 66, no. 12, pp. 9248–9259, Dec. 2019.

Cikai Ye (S'16) received the B.Eng. degree in electrical engineering from Zhejiang University, Hangzhou, China, in 2013. Since 2015, he has been working toward the Ph.D. degree with the Department of Electrical and Computer Engineering, National University of Singapore, Singapore.

From 2013 to 2015, he worked as a Hardware Engineer with Holland Royal Philips, Lighting, R&D, Shanghai, China. His research interests include LED drivers for lighting, and ac–dc and dc–dc power converters.

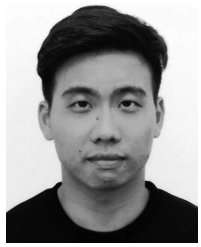

Hao Wei Chan received the B.Eng. degree in electrical engineering from the National University of Singapore, Singapore, in 2019.

Since 2019, he has been working as an Electrical Engineer with SP Group, Singapore. His research interests include LED drivers and power converters.

Dongdong Lan (S'16) received the B.Eng. degree in electrical engineering from Xian Jiaotong University, Xian, China, in 2015. He was also an Exchange Student with National Tsing Hua University in 2013. Since 2015, he has been working toward the Ph.D. degree with the Department of Electrical and Computer Engineering, National University of Singapore, Singapore.

His research interests include power converters for more electric aircraft, matrix converter, and ac–dc and dc–dc power converters.

Pritam Das (S'09–M'12–SM'13) received the M.A.Sc. and Ph.D. degrees in electrical engineering from the University of Western Ontario, London, ON, Canada, in 2005 and 2010, respectively.

From 2010 to 2011, he was a Postdoctoral Fellow with the Queen's Centre for Energy and Power Electronics Research (ePOWER), Queen's University, Kingston, ON, Canada, and with PE consultants, Kingston.

From 2011 to 2013, he was with Murata Power Solutions, Toronto, ON, Canada, as an Electrical Design Engineer. From 2013 to 2017, he was an Assistant Professor with the Department of Electrical and Computer Engineering, National University of Singapore, Singapore. He is currently an Assistant Professor with the Department of Electrical and Computer Engineering, State University of New York, Binghamton, NY, USA. His present research interests include wide band gap device-based single-stage high power resonant converters for behind-the-meter grid-connected energy storage systems, dc Data Centers, ac fast chargers for heavy electric vehicles, reliable modular multi-level converters for off-shore wind power and energy storage systems, high power and high efficiency electrolytic capacitor free long life time centralized multi-channel LED driver with selective deep dimming capabilities, etc. He has applied two U.S. patents and has published more than 80 technical papers in refereed journals and conferences.

Dr. Das is an Associate Editor of IEEE TRANSACTIONS ON INDUSTRIAL ELECTRONICS. He is also a Reviewer for IEEE TRANSACTIONS ON POWER ELECTRONICS, and IEEE TRANSACTIONS ON INDUSTRIAL INFORMATICS. He also founded PowerEff, a power solutions company for commercializing high-power LED drivers.

Sanjib Kumar Sahoo (S'01–M'08–SM'12) received the B.Tech. (Hons.) degree from the Indian Institute of Technology, Kharagpur, India, in 1993, and the Ph.D. degree from the National University of Singapore (NUS), Singapore, in 2007, both in electrical engineering.

He worked in industry from 1993 to 2001. In 2001, he worked as a Research Scholar with the Department of Electrical and Computer Engineering, NUS, where he currently works as a Senior Lecturer. He has led teams for developing and teaching new project-based modules at the undergraduate level. His research interests include the development of high-performance controllers for motor drives, and power converters for grid interfacing of renewable energy sources, using advanced nonlinear and intelligent control techniques.